Tectonophysics, 43 (1977) 257—291

SUPERPLASTIC FLOW IN FINEGRAINED LIMESTONE

S.M. SCHMID *, J.N. BOLAND and M.S. PATERSON

Research School of Earth Sciences, Australian National University, Canberra, A.C.T. (Australia)

(Submitted September 22, 1976; revised version accepted March 7, 1977)

ABSTRACT

Schmid, S.M., Boland, J.N. and Paterson, M.S., 1977. Superplastic flow in finegrained limestone. Tectonophysics, 43: 257—291.

Creep of Solnhofen limestone at temperatures between 600° and 900°C was found to fall into three different flow regimes: regime 1 with an exponential stress-dependence of strain rate, regime 2 with power-law creep and $n \sim 4.7$ and finally a superplastic regime 3 with $n \sim 1.7$. Within the superplastic regime the creep behaviour is strongly grain-size dependent, the strain rate increasing markedly with decrease in grain size at a given stress. Microstructural observations indicate that in regimes 1 and 2 intracrystalline plasticity is dominant whereas the superplastic regime is characterized by grain-boundary sliding. The crystallographic preferred orientation within the superplastic regime is weaker and of different geometry when compared with that in flow regimes 1 and 2. In a discussion on the deformation mechanisms it is suggested that flow regimes 1 and 2 are regimes of dislocation creep in which the rate controlling step is diffusion assisted; for the superplastic regime existing models of grain-boundary sliding are compared with the observations. Finally, the tectonophysical importance of superplasticity is discussed and by extrapolating the observed creep behaviour to geological strain rates it is found that superplasticity in rocks is to be expected under a wide range of conditions, particularly at small grain sizes.

INTRODUCTION

Polycrystalline aggregates can deform by a wide variety of mechanisms and as a consequence there are various constitutive equations for creep relating the strain rate to the flow stress (Stocker and Ashby, 1973a; Weertman, 1975). The deformation mechanisms observed at elevated temperatures ($T/T_m > 0.4$ where T_m is the absolute melting point) can be subdivided into three main categories: (1) flow involving the motion of dislocations ("dislocation glide" and "dislocation creep" in the terminology by Stocker and Ashby, 1973a); (2) diffusional creep (for example Nabarro-Herring and Coble creep); and (3) grain-boundary sliding mechanisms.

---

* Now at Geologisches Institut der ETH, Zurich, Switzerland.

In any particular situation, the flow regime defined by the mechanism and its associated flow law is mainly determined by the deviatoric stress level on the one hand and by the combination of temperature and strain rate on the other hand. There is, however, a serious problem of relating the flow regime in a tectonophysical situation of slow strain rates with the flow regimes attainable in the laboratory. Fortunately, the combined influence of temperature and strain rate allows deformation mechanisms typical of slow strain rate, low stress environments to be studied at laboratory strain rates if temperatures higher than the ones expected in nature are used (Paterson, 1976a). This approach has been adopted in the present study of the flow behaviour in Solnhofen limestone using relatively high temperatures of 600—900°C (T/T_m = 0.54—0.73), temperatures above those to be expected naturally in crustal environments where limestones are abundant.

It is known that a small grain size favours diffusional creep and grain-boundary sliding mechanisms under stress—temperature conditions where dislocation creep would otherwise dominate. With this influence of grain size in mind the Solnhofen limestone (grain size 4 μm) was chosen as a test material. The flow behaviour of the coarse-grained (300 μm) Yule marble under similar temperatures was already well known from the work of Heard and Raleigh (1972).

It was found that the Solnhofen limestone, at the higher temperatures and lower strain rates, exhibited a number of flow and structural characteristics typical of so-called superplasticity in metals and alloys. Superplasticity, as used in relation to metals, refers to exceptional ductility in tensile tests, whereby elongation can exceed 1000% without necking and subsequent failure. It can be observed at temperatures $>0.5\ T/T_m$. The term superplasticity does not imply or even define a particular deformation mechanism. However, most authors (see recent review by Edington et al., 1976) regard grain-boundary sliding as an important aspect of the deformation mechanism in superplastic flow; the intragranular deformation mechanisms mentioned above do not satisfactorily explain many observed rheological and structural features.

Although the extreme ductility in extension is the primary characteristic of superplastic flow, it is clearly a criterion which is of little use in the geological context or even in experimental rock deformation where compressional tests are usually performed. A number of other characteristics of superplastic flow can be cited, such as:

— The value of n in a constitutive equation of the form $\dot{\varepsilon} \propto \sigma^n$ is low, with $1 < n < 3$.

— The grains remain approximately equiaxed even after large amounts of strain, and a small grain size (usually <10 μm) seems to be a condition for superplasticity in the laboratory.

A geological example of superplasticity has been inferred by Boullier and Gueguen (1975) from a microstructural study on mylonites.

A preliminary account of the rheological observations that revealed the

transition to superplasticity in Solnhofen limestone has already been published (Schmid, 1976). Here, we give further data to consolidate this evidence, add observations from optical, electron-microscope and preferred-orientation studies and discuss the mechanisms involved. Finally, the relevance of superplastic deformation in geological environments will be discussed.

APPARATUS AND TECHNIQUE

All specimens were deformed in compression under a confining pressure of 3 kbar, using a high-pressure, high-temperature apparatus built and described by Paterson (1970, 1976b). This apparatus has the following characteristics:

— Gas confining medium. No correction for the strength of the confining medium has to be made.

— Internal load cell, directly measuring the axial load inside the pressurized confining medium. No corrections for friction at the pistons has to be made. Loads of less than 5 kg (corresponding to 6 bar on 10 mm diameter specimens) can be detected.

— Internal furnace with two separately controlled windings. By suitably balancing the power in upper and lower winding the temperature gradient over the specimen can be minimized to within ±5°C of the nominal temperature.

Cores of 10 mm diameter and 20 mm length were drilled from a block of Solnhofen limestone perpendicular to bedding. After oven-drying the cylinders were sealed in copper jackets of 0.25 mm wall thickness.

At very low flow stresses the strength of the jacket makes a substantial contribution to the total load sustained by the assembly (copper is stronger than Solnhofen limestone at 900°C and the lowest strain rates!). Therefore, the strength of the copper was determined in a series of copper specimens at various temperatures and strain rates in order to make accurate corrections for the copper strength. The usual additional corrections for apparatus distortion and cross-section increase of the specimen were made in deriving the stress—strain curves.

Most of the tests were run at constant displacement rate, corresponding to constant strain rate when steady-state flow is reached. Additional tests, such as stress relaxation, variable strain rate and creep (constant stress) tests, were also performed.

After straining, the temperature was immediately lowered in order to minimize annealing of the structure and to stop additional grain growth.

Calcite would decompose rather rapidly at the highest test temperatures under ambient pressures. Since the specimens were sealed off and kept at a confining pressure of 3 kbar, substantial decomposition was avoided by the CO_2 pressure building up inside the jacket after only minor amounts of calcite decomposed; the amount of this damage appeared to be negligible. The

limestone was deformed within the stability field of calcite.

For optical studies prepolished ultra-thin sections were prepared from a cut containing the axis of shortening. Relatively big areas of a specimen could be studied at a thickness of one or a few microns (grey first order in calcite under crossed polarizers).

The crystallographic preferred orientation of several crystallographic planes was measured in a Philips PW 1078 texture goniometer mounted on a Philips X-ray diffractometer PW 1050. Because axial symmetry of the fabric, corresponding to the symmetry of the experimental conditions, can be assumed (Wenk et al., 1973), X-ray intensities were only measured in transmission and for grains with reflecting planes normal to the 50 μm thick slab of material cut in a plane containing the axis of shortening.

The slab was rotated by 540° in the angle χ about its normal axis, giving six measurements of the basic 90° interval of the transmission profile. The relative intensities above the background were read off at 4.5° intervals in χ, averaged and normalized to express the degree of preferred orientation following the procedure described by Means and Paterson (1966) and Baker et al. (1969). The multiples of a uniform distribution so obtained correspond to the pole densities as they would be obtained by optical methods for a uniform grain size; for example, a normalized maximum concentration of 2.0 at an angle of 30° would correspond to a maximum with 2% of poles per 1% area distributed over a girdle at an angle of 30° to the direction of shortening.

Scanning and transmission-electron microscopy (SEM and TEM) were used to investigate microstructural features in the deformed specimens. SEM studies — using a Cambridge Stereoscan 180 — were made on the surfaces of split cylindrical specimens that had been prepolished down to 0.25 μm diamond, the surfaces being separated by an 0.03 mm gold foil during the deformation run (split-cylinder technique, Heard and Raleigh, 1972). Many attempts were made to inscribe fiducial lines into the surface in order to measure the offsets at grain boundaries produced by sliding. Fine scratches did not survive the deformation experiment presumably because surface diffusion rates were sufficiently rapid to obliterate the scratches. In another unsuccessful approach, a grid outline was made by evaporating carbon through a copper grid but the carbon film tended to buckle or crack rather than follow the deformation of the calcite.

The method that gave the most convincing evidence for grain-boundary sliding was stereoscopic observation of the surfaces. The vertical height difference between neighbouring grains, v_r, was calculated from parallax measurements using a folding mirror stereoscope (Boyde, 1970). The strain due to grain-boundary sliding e_{gbs} was calculated from the average $\bar{v}_r$, using (Langdon, 1976) $e_{gbs} = \phi \bar{v}_r/d$, where ϕ is a geometrical factor (~1.1) and d the average grain size.

For TEM studies samples from the central region of the specimen were thinned by ion bombardment (Barber, 1970; Gillespie et al., 1971) and

examined in a JSEM 200 electron microscope operating at 200 kV. Dislocation densities were determined by the line-intercept method (Hale, 1974); the greatest uncertainty arises from assigning an average foil thickness.

RHEOLOGY AND CONSTITUTIVE EQUATIONS FOR FLOW

Constant strain-rate tests

Over the entire range of test conditions the flow stress reached a practically constant (steady state) level after a few percent strain (Fig. 1), even when the fastest strain rate (10% strain in 16 seconds) was applied. Slight but systematic departures from this steady-state behaviour were only observed at the highest temperatures and slowest strain rates, where the flow stress kept rising with increasing strain (Fig. 1). This apparent work hardening is puzzling at first sight because it would normally be expected at the lowest temperatures and fastest strain rates. In this case, however, it is believed to arise from grain growth during deformation leading to an increase in flow stress. The influence of grain size on the strength of this rock will be discussed in a later section.

The results of the constant strain-rate experiments are listed in Schmid

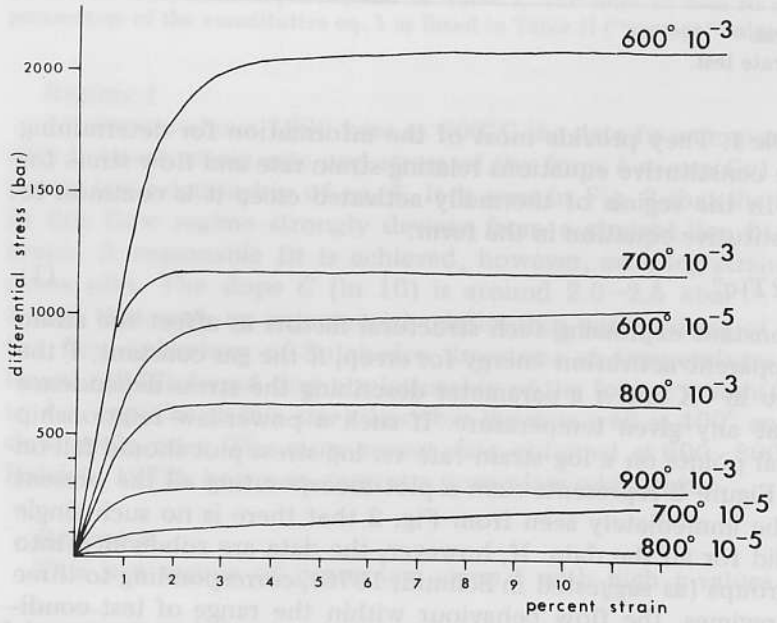

Fig. 1. Stress—strain curves for Solnhofen limestone deformed under various conditions of temperature and strain rate and under 3 kbar confining pressure.

TABLE I

Complementary list of experiments (new experiments not published by Schmid, 1976)

Run number	Temp. (°C)	Strain rate	Differential stress	Flow regime
2674 *	700	$1.0 \cdot 10^{-3}$	1021	2
2793 *	800	$1.1 \cdot 10^{-4}$	217	3
2802 *	800	$1.1 \cdot 10^{-4}$	150	3
2795 *	800	$1.0 \cdot 10^{-4}$	145	3
2678 *	800	$7.4 \cdot 10^{-5}$	115	3
2668 *	800	$7.1 \cdot 10^{-5}$	117	3
2851 *	800	$3.3 \cdot 10^{-5}$	86	3
2882	800	$3.2 \cdot 10^{-5}$	93	3
2702 *	800	$3.1 \cdot 10^{-5}$	71	3
2762	800	$1.1 \cdot 10^{-5}$	39	3
2762 **	800	$1.0 \cdot 10^{-6}$	10 (11.0%)	3
2710 **	900	$4.8 \cdot 10^{-4}$	99 (13.0%)	3
2710	900	$2.5 \cdot 10^{-4}$	57	3
2708 **	900	$2.3 \cdot 10^{-4}$	105 (13.0%)	3
2708	900	$1.2 \cdot 10^{-4}$	51	3
2709 **	900	$1.2 \cdot 10^{-4}$	68 (14.7%)	3
2902	900	$9.9 \cdot 10^{-5}$	29	3
2709 **	900	$7.3 \cdot 10^{-5}$	49 (12.4%)	3
2709 **	900	$4.0 \cdot 10^{-5}$	31 (11.6%)	3
2709	900	$2.1 \cdot 10^{-5}$	24	3
2717	900	$1.1 \cdot 10^{-5}$	10	3

* Split-cylinder test.
** Variable strain-rate test.

(1976) and Table I. They provide most of the information for determining the form of the constitutive equations relating strain rate and flow stress for this limestone. In the region of thermally activated creep it is common to present the constitutive equation in the form:

$$\dot{\epsilon} = A \exp(-H/RT)\sigma^n \qquad (1)$$

where A is a constant expressing such structural factors as affect the strain rate, H is the apparent activation energy for creep, R the gas constant, T the test temperature in °K and n a parameter describing the stress-dependence of strain rate at any given temperature. If such a power-law relationship holds, isothermal points on a log strain rate vs. log stress plot should fall on a straight line. Figure 2 represents such a plot incorporating all the present results. It can be immediately seen from Fig. 2 that there is no such single relationship valid for all the data. If, however, the data are subdivided into the following groups (as suggested in Schmid, 1976), corresponding to three different flow regimes, the flow behaviour within the range of test conditions reported here can be adequately described by three sets of constitutive equations.

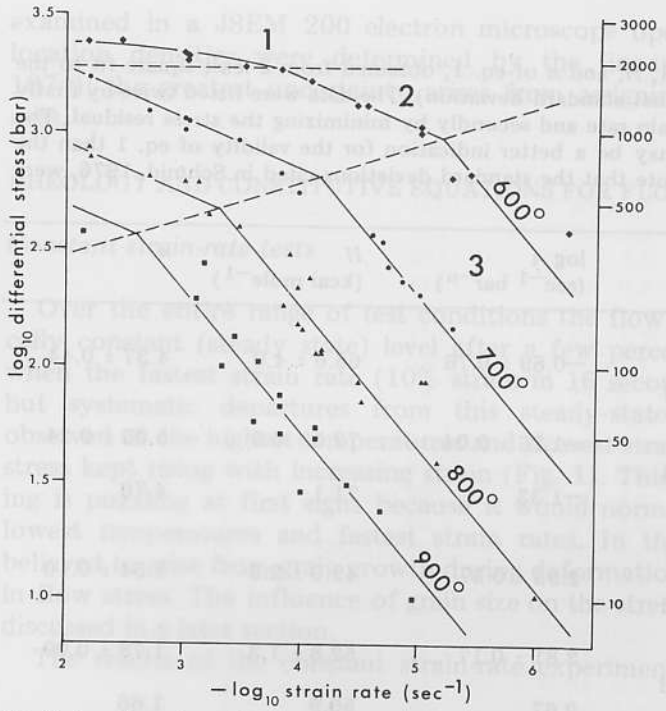

Fig. 2. Log-log plot of the differential stress at 10% strain vs. the strain rate of all experiments listed in Schmid (1976) and in Table I. The lines of best fit correspond to the parameters of the constitutive eq. 1 as listed in Table II ("average" values).

Regime 1

At stresses above 1900 bars at 600°C the data fit an exponential relationship between strain rate and stress of the form $\dot{\epsilon} \propto \exp(C\sigma)$ better than the power-law relationship of eq. 1. It is seen in Fig. 2 that the few data points in this flow regime strongly deviate from a straight line fit on this log-log graph. A reasonable fit is achieved, however, on a log strain rate vs. linear stress plot. The slope C (ln 10) is around 2.0—2.5 kbar^{-1}. Rutter (1974) found that such an exponential relationship with a slope of 2.7 kbar^{-1} fits the flow behaviour of Solnhofen limestone at temperatures below 600°C. Heard (1963) found that a relationship of the form $\dot{\epsilon} \propto \sinh(C\sigma)$ (equivalent to $\dot{\epsilon} \propto \exp(C\sigma)$ in this case) describes the data well at 400° and 500°C at the slow strain rates. The more recent data obtained at 600—800°C (Heard and Raleigh, 1972), however, suggest a power-law relationship.

Regime 2

This is a regime of power-law creep * with high n-values near 5 and an

* An extension of the exponential relationship of regime 1 into regime 2 was rejected because of the poor fit obtained by initially plotting all the data of regimes 1 and 2 on a log strain rate vs. stress plot.

TABLE II

Values for parameters log A, H, and n of eq. 1, obtained from a least-square fit to the logarithmic form of eq. 1 (first standard deviation). The data were fitted twice by firstly minimizing deviations in strain rate and secondly by minimizing the stress residual. The high degree of agreement may be a better indication for the validity of eq. 1 than the standard deviations cited (note that the standard deviations cited in Schmid, 1976, were erroneously overstated)

		log A (sec^{-1} bar^{-n})	H (kcal $mole^{-1}$)	n
Flow regime 2	strain-rate residual minimized	−0.89 ± 0.76	68.6 ± 4.0	4.37 ± 0.44
	stress residual minimized	−1.76 ± 0.04	73.5 ± 0.9	5.03 ± 0.24
	average	−1.33	71.1	4.70
Flow regime 3	strain-rate residual minimized	2.53 ± 0.37	49.0 ± 2.3	1.54 ± 0.10
	stress residual minimized	2.81 ± 0.17	52.8 ± 1.3	1.78 ± 0.09
	average	2.67	50.9	1.66

apparent activation energy for creep of about 70 kcal $mole^{-1}$ (Table II). The stress for transition into a regime with lower n-values (regime 3 described below) is clearly temperature-dependent and rises from 300 bars at 900°C to 1000 bars at 600°C. The boundary between regimes 2 and 3 was located by making a first fit omitting the data in the apparent transition region, then assigning these data to the respective regimes thus provisionally determined, and finally optimizing with a least-squares fit using all the data (Table II).

The value of parameter n found in this regime is compatible with values for n found in a variety of materials including rocks (Carter, 1975) and there exists a number of models based on the motion of dislocations which predict n-values in the region of 3 to 5 (Weertman, 1975; Stocker and Ashby, 1973a; Kirby and Raleigh, 1973). It is interesting to note, however, that Yule marble (Heard and Raleigh, 1972) shows an exceptionally high n-value, around 8. Since the main difference between Solnhofen limestone and Yule marble lies in the grain size (300 μm in Yule marble) it can be suspected that the difference in n-values has to be attributed to some grain size effect.

Regime 3

At the lowest stresses exceptionally low n-values (around 1.7) and a lower

activation energy for creep (around 50 kcal mole^{-1}) are derived from the data (Table II). Such low n-values are characteristic of superplastic flow especially when taken in conjunction with structural observations presented below.

It must be emphasized that only for the sake of obtaining a simple form of a constitutive equation for creep, useful for extrapolations into geological environments, was a single set of parameters A, n and H assumed for the entire regime 3. The relaxation tests described below suggest that the parameter n representing the stress-dependence of strain rate actually decreases continuously with the stress towards a minimum only slightly greater than unity. Many superplastic materials show a sigmoidal form of the log stress—log strain rate curve; that is, after a decrease from n-values >3 into a region of $1 < n < 3$ (superplastic regime) n increases again as the flow stress and the strain rate decrease further. There is no indication that the n-value increases again at the lowest stresses in Solnhofen limestone, however, and a threshold stress, if existent for this material, must lie well below 10 bars.

The influence of grain size

A study by Olsson (1974) on various calcite rocks of different grain sizes showed that in the temperature range of 25—300°C the yield stress increases with decreasing grain size according to $\sigma_y = \sigma_o + Kd^{-1/2}$, where σ is the yield stress, d the grain size, σ_o and K are constants (Petch, 1953). A comparison of strength at 10% strain between Solnhofen limestone and coarser grained Yule marble (Heard and Raleigh, 1972) at any given laboratory conditions where Solnhofen limestone deforms in flow regime 2 shows that the fine-grained limestone is stronger than Yule marble. This extends such a grain-size dependence of the strength into temperatures >300°C. This behavior probably reflects the influence of the grain boundaries on the free movement of dislocations within the grains. Expressed alternatively in terms of strain compatibility problems at grain boundaries, a higher density of grain boundaries raises the stress necessary to accommodate slip in every grain of the aggregate. This grain-size dependence, however, is relatively weak when compared with the much stronger effect of grain size now to be described and it can be neglected to a first approximation.

If a comparison is made with Yule marble (Heard and Raleigh, 1972) under conditions where Solnhofen limestone deforms superplastically it is to be noted that Solnhofen limestone becomes dramatically weaker than Yule marble. At 800°C and a strain rate of 10^{-5} sec^{-1} Yule marble is approximately six times stronger than Solnhofen limestone (260 bars as compared with 41 bars in Solnhofen limestone). This very strong grain-size dependence in the opposite sense to that described above suggests that grain-boundary sliding and/or diffusional flow must be operative in the superplastic regime 3 for Solnhofen limestone. Both these mechanisms favour lower flow stresses at smaller grain sizes. In contrast to the case of intracrys-

talline slip (regime 2) a high density of grain boundaries now leads to a lower flow stress because grain boundaries are potential sites of intercrystalline sliding and/or enhanced diffusion rates.

The grain-size dependence in superplasticity is usually described by the relation $\dot{\varepsilon} \propto d^{-b}$ at constant stress, where d is the grain size and b a constant with values between 2 and 3 (Edington et al., 1976). An attempt has been made in this study to establish experimentally such a relationship and to evaluate the parameter b with a series of additional tests, listed in Fig. 3.

As will be shown in the section 'Optical microscopy' grain growth occurs in Solnhofen limestone at the higher temperatures. By annealing at temperatures higher than the test temperature a series of specimens of various grain sizes was produced. All the specimens were subsequently deformed at 800°C and at the strain rate $3 \cdot 10^{-5}$ sec^{-1}. Figure 3 shows the flow stresses at 10% strain as a function of the grain size. The data point labelled "best fit" is at the stress predicted by the constitutive equation for superplastic flow listed in Table II ("average" values) and at the average grain size in this flow regime (5.9 μm). It is apparent from Fig. 3 that the flow stress is extremely sensitive to grain size at the grain sizes <10.5 μm and that this sensitivity is very weak at the grain sizes >10.5 μm. This suggests that, at the larger grain sizes, grain-size independent dislocation creep becomes at least competitive with superplastic flow.

Unfortunately, the grain-size interval from 5.9 to 10.5 μm is too small to allow for an accurate determination of constant b in the relationship $\dot{\varepsilon} \propto d^{-b}$. Therefore, instead of calculating a best fit to the five data points in this

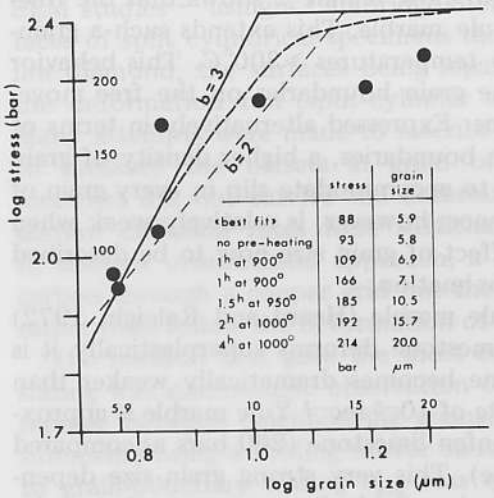

Fig. 3. Graph illustrating the influence of grain size on the strength of specimens equilibrated to different grain sizes by annealing. Straight lines: prediction if $\dot{\varepsilon} \propto d^{-b}$ holds in the superplastic regime; curved broken line: prediction for the same relationship in the superplastic regime but assuming the strain rates in flow regimes 2 and 3 to be additive.

grain-size interval the predicted trends for $b = 2$ and $b = 3$ are superimposed in Fig. 3, calculated as follows.

By introducing the grain size as an independent parameter and assuming that the best-fit equation in Table II (regime 3) is valid for an average grain size of 5.9 μm the constitutive equation for superplastic flow was expanded into:

$$\dot{\epsilon} = A^* d^{-b} \exp(-H/RT)\sigma^n \tag{2}$$

where $\log A^*$ is equal to 4.21 and 4.98 when sec, bar and μm are used and $b = 2$ and 3 respectively. This constitutive equation was then used to calculate the sloping lines in Fig. 3 for stresses within the superplastic regime. For the larger grain sizes, the predicted stress derived by using the parameters for flow regime 2 (Table II), taken as grain-size independent, was found to be lower. This is graphically expressed by the horizontal line in Fig. 3, truncating the lines for regime 3 at a point in stress—grain size space where the deformation mechanism changes (compare also Fig. 2). It is seen that the predicted grain size at which the stress becomes grain-size independent (10.5 μm) as well as the data points at grain sizes <10.5 μm are reasonably well reproduced by this approach. The stresses observed at grain sizes >10.5 μm are lower than predicted, but this discrepancy is partly removed if the two mechanisms are assumed to be additive (curved line). Although a value of 2 for parameter b in the superplastic regime cannot be rejected entirely on the basis of these few data, a value of 3 rather than 2 for b is favoured. The consequences of this choice in a geological context will be discussed in the section 'Tectonophysical significance'.

Creep and stress-relaxation tests

Stress—strain curves obtained from constant strain-rate tests within regime 2 and regime 3 are similar in shape (Fig. 1). Creep curves obtained under constant stress, however, are able to reveal differences as shown in Fig. 4. In both tests the same steady-state strain rate is finally approximated. In test 2660 (600°C, 1315 bars) the specimen was deformed within regime 2 characterized by high n-values; the initially very high strain rate steadily dropped (primary creep) and after 3% creep strain steady state was established. In the case of test 2654 (700°C, 370 bar) deformed under superplastic conditions steady state was almost immediately established after a short strain interval with only slightly higher strain rates.

At the end of many of the constant strain-rate tests, stress-relaxation tests were performed. They have been reported earlier (Schmid, 1976) where it was shown that the tests represent a valuable alternative for establishing the constitutive equation of creep. Its validity rests on the demonstration that the rheological behaviour revealed momentarily at any given stress level during a relaxation run is identical with the rheology inferred from a series of constant strain-rate experiments under conditions of steady state at the same stress levels. This observation indicates that the specimen continuously

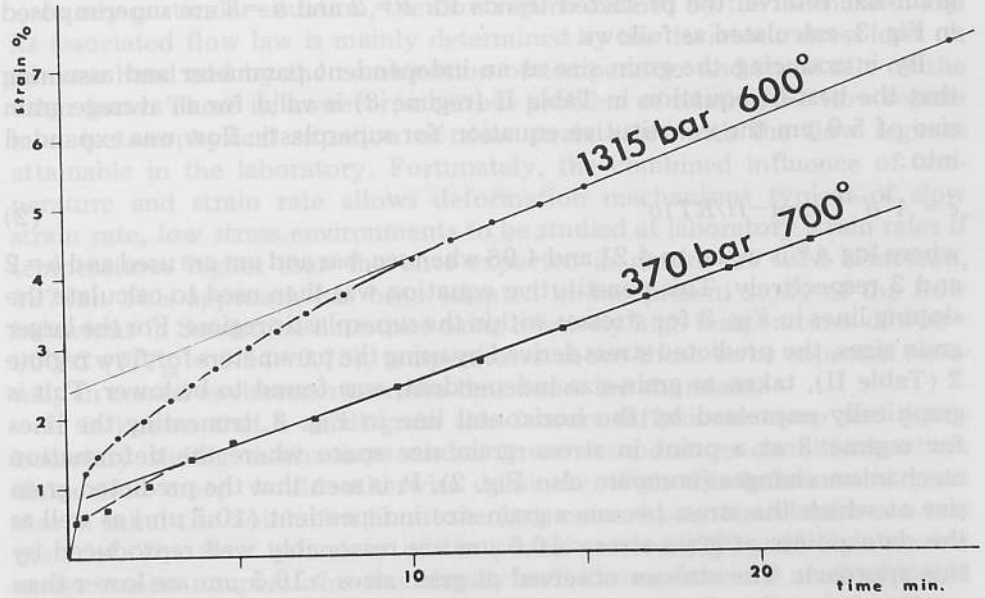

Fig. 4. Creep curves for test 2660 (flow regime 2, 600° C) and test 2654 (flow regime 3, 700° C), both leading to a steady-state strain rate of approximately $3 \cdot 10^{-5}$ sec^{-1}. Note the very weakly developed region of transient creep in the 700° C (superplastic) run.

adjusts to a steady state or at least its close approximation as the stress drops. Since the behaviour is not yet adequately understood theoretically caution must be applied in extending this finding to other materials.

A practical advantage of the relaxation method is that a great range of stresses is scanned within a single test and this enables one to obtain information on minor changes in the stress dependence of the strain rate as described by parameter n in eq. 1. This fact is exploited by plotting the value of parameter n as obtained from relaxation tests run within the superplastic flow regime against the flow stress. It can be shown that the value n in a stress-relaxation test is given by:

$$n = \frac{\partial \log(\mathrm{d}\sigma/\mathrm{d}t)}{\partial \log \sigma}$$

or approximated between two discrete points A and B on a relaxation curve by:

$$n = \frac{\log(\mathrm{d}\sigma/\mathrm{d}t)_A - \log(\mathrm{d}\sigma/\mathrm{d}t)_B}{\log \sigma_A - \log \sigma_B}$$

Although considerable scatter exists in Fig. 5, where n is plotted against

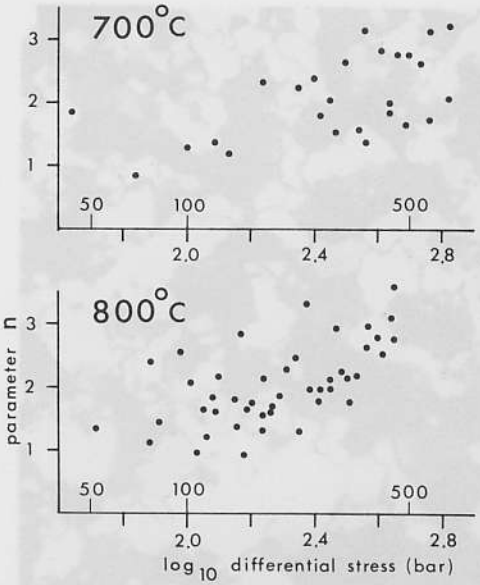

Fig. 5. Plot of the parameter n, as obtained from stress-relaxation tests, against the logarithm of the differential stress at 700° C and 800° C within the superplastic regime.

the logarithm of the flow stress between such points A and B as obtained from several relaxation tests, a trend for n-values to decrease with decreasing stress emerges. This indicates that the assumption of a constant parameter n within the superplastic flow regime is a simplification and that n in fact steadily decreases with decreasing stress.

MICROSTRUCTURE

Optical microscopy

Figure 6 shows the microstructures of Solnhofen limestone undeformed (Fig. 6a), and after deformation in flow regime 2 (high n-values, Fig. 6b) and in flow regime 3 (superplastic regime, Fig. 6c). The undeformed limestone has a considerable scatter in grain size and the grain boundaries are serrate.

In flow regimes 1 and 2 flattening of grains and effects of intragranular plasticity such as undulose extinction and subgrain boundaries are observed (Fig. 6b). Detailed work on the nature of these deformation features is not possible with light optics because of the very small grain size. The serrate character of grain boundaries is largely retained.

Figure 6c shows the drastically different microstructure of a superplastically deformed specimen. Although this specimen was shortened by roughly the same amount as the specimen of Fig. 6b, the grains remained almost

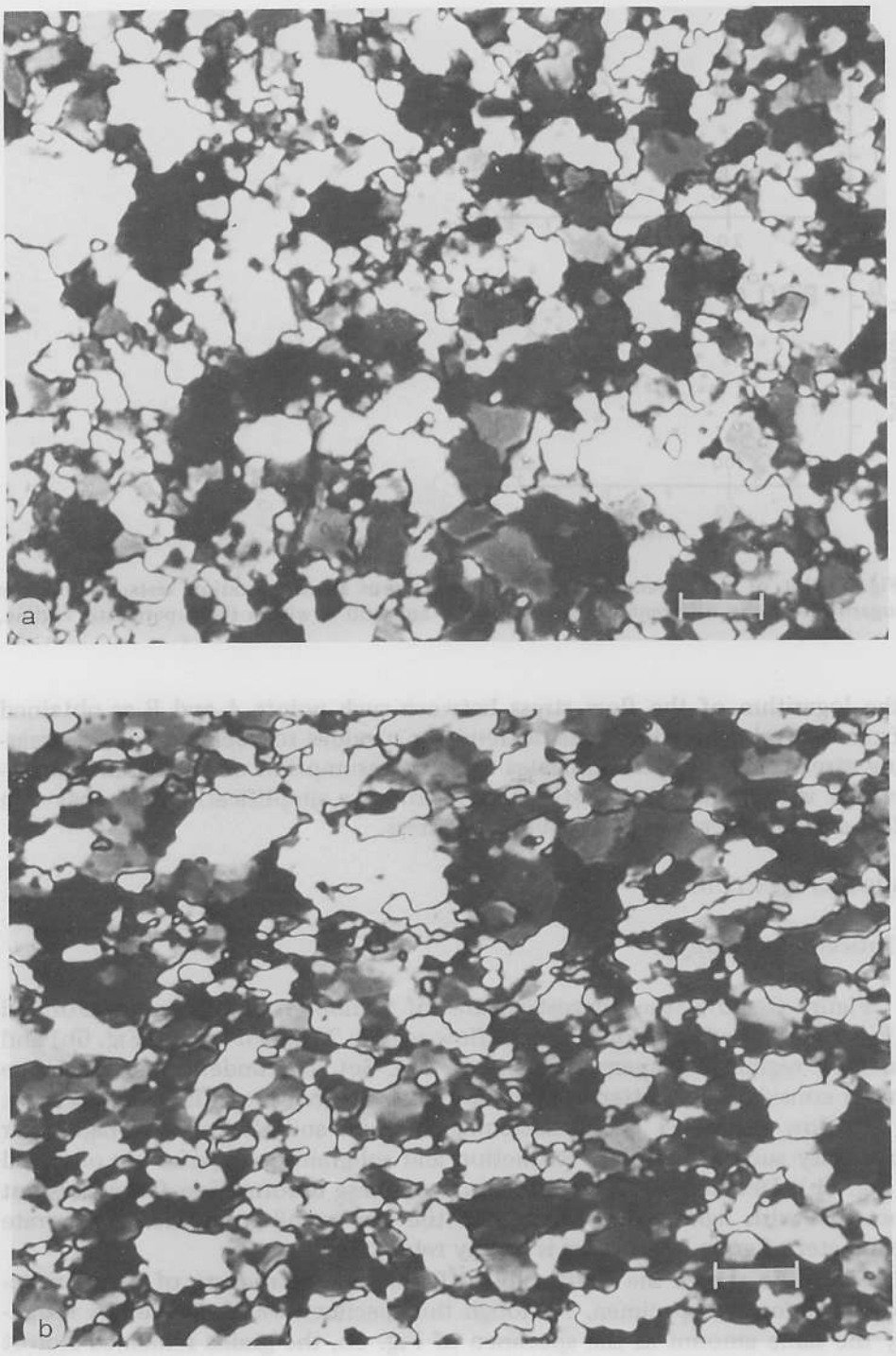
a
b

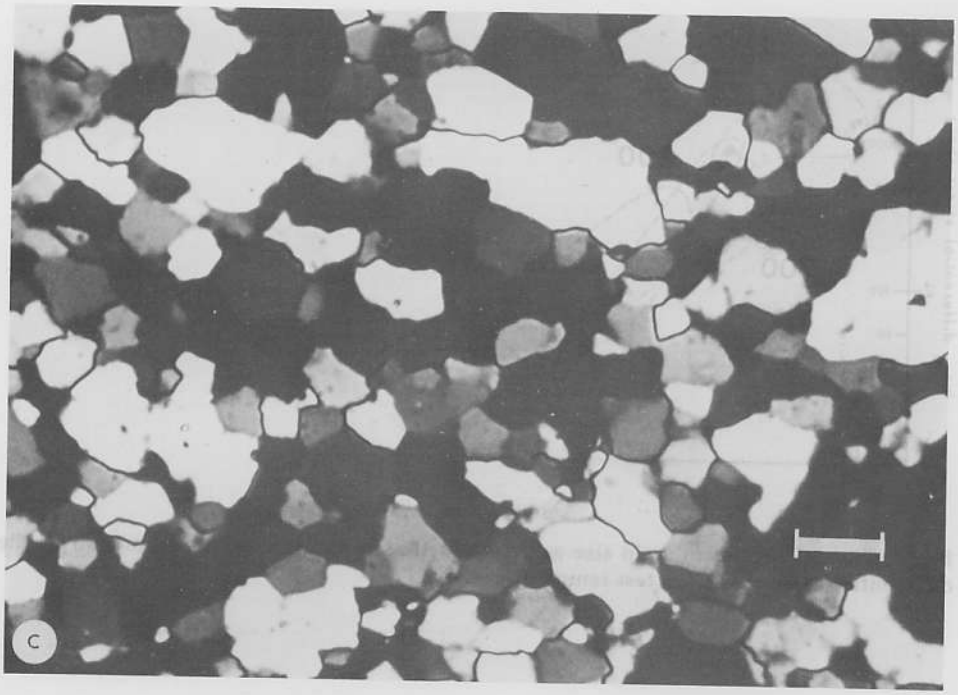

Fig. 6. Photomicrographs of ultra-thin sections, crossed polarizers, scale: 10 μm. (a) Solnhofen limestone, undeformed. Mean grain size: 4.2 μm. (b) Solnhofen limestone, deformed in flow regime 2 (run 2632, 700 °C, $2 \cdot 10^{-3}$ sec^{-1}, 31% shortening, 4.8 μm). (c) Solnhofen limestone, deformed in the superplastic flow regime (run 2569, 900°C, $6.7 \cdot 10^{-4}$ sec^{-1}, 36% shortening, 5.4 μm).

equiaxed. The grain boundaries are straight and the resulting polygonal structure clearly indicates that grain-boundary migration must have occurred. Some grain growth resulted too but because of the polygonal microstructure the amount of relative grain growth is easily over-estimated at first sight.

Twinning is extremely rarely observed in any of the deformed specimens.

Systematic measurements of grain size and amount of flattening were made on a number of deformed specimens. The results are graphically summarized in Figs. 7 and 8 and will now be discussed in turn.

Grain size

The grain size was measured by counting the number of grain boundaries crossing marker lines run in a grid through the photomicrographs parallel and perpendicular to the direction of shortening; a sample of approximately 1000 grains was taken. Where grain flattening occurred the grain size is defined as the arithmetric mean of the grain size as determined parallel to the mutually perpendicular marker lines. The starting material has a mean grain size of 4.1 μm and Fig. 7 illustrates the range of observed grain sizes

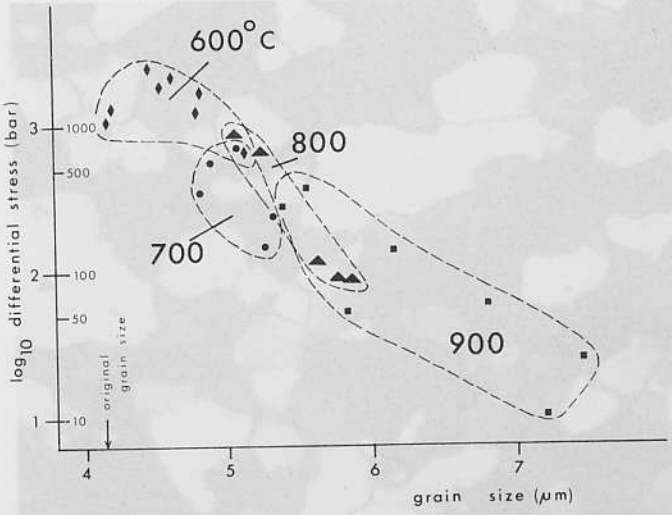

Fig. 7. Plot of the mean grain size as determined after the test vs. the logarithm of the differential stress at various test temperatures.

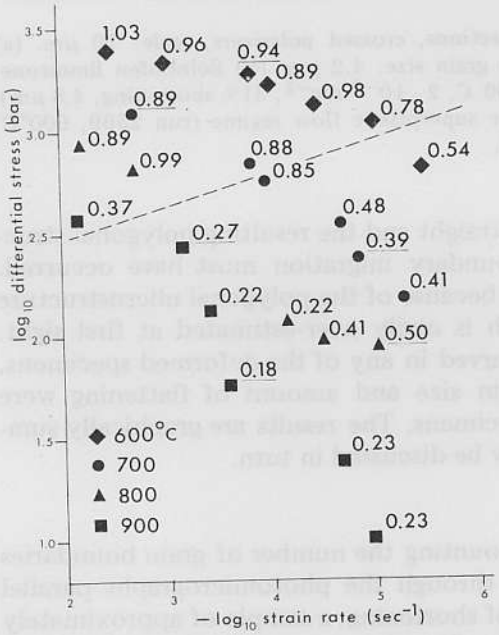

Fig. 8. The ratio of e_g (the strain inferred from the amount of grain flattening) over e_t (the total strain applied) for various data points plotted in a log-log graph of differential stress vs. strain rate (compare Fig. 2); broken line indicates the transition from flow regime 2 into flow regime 3 as inferred from Fig. 2. Underlined numbers: $e_t > 20\%$.

after deformation (4.1 to 7.5 μm) versus the logarithm of the differential stress at which the specimens were deformed.

Groups of data for deformation at the same temperature as well as the total data show a tendency for the grain size to increase with decreasing stress; a similar trend was pointed out by Kohlstedt et al. (1976) for olivine. Although this trend suggests a direct relationship between grain size and stress, it has to be kept in mind that a specimen deformed at a lower stress has been for a longer period of time at the test temperature because of the lower strain rate applied. This grain size—stress relationship might, therefore, partly reflect the amount of grain growth as a function of time at any given temperature regardless of the stress applied.

It is interesting to note that, whereas some grain growth occurs in the finegrained Solnhofen limestone under our experimental conditions, grain-size reduction occurs in coarse-grained marble (Heard and Raleigh, 1972) and in the matrix of an oolitic limestone (Schmid and Paterson, 1977) under the same conditions. This suggests that the grains in a calcite aggregate tend to approach an equilibrium size during deformation at elevated temperatures although it is not clear which experimental variables determine this equilibrium grain size nor how the size varies with change in experimental conditions.

Grain flattening

The average aspect ratio R of grains was determined with the same method as used for the grain size and is simply defined as the ratio of the grain size as measured parallel to the direction of shortening over the grain size as measured in a perpendicular direction. If the average grain is assumed to be spherical initially, with unit diameter, and if the maximum and minimum diameters of the spheroid into which it is deformed are $(1 + e_1)$ and $(1 + e_3)$ respectively, then, for the constant volume condition $(1 + e_3)\,(1 + e_1)^2 = 1$, it follows that the engineering strain in the direction of shortening as indicated by the flattening of grains (e_g) is given by:

$$e_3 = e_g = R^{2/3} - 1 \text{ where } R = \frac{(1 + e_3)}{(1 + e_1)}$$

The amount of shortening, e_g, as inferred from the amount of grain flattening, is only an approximate measure of the amount of strain produced by intracrystalline plasticity, because sources of errors result from:

(1) The constant volume assumption. This does not strictly hold because an unknown amount of grain growth occurs during straining of the specimen. However, the specimens have been equilibrated at the test temperature for at least 30 minutes and, during this time, most of the grain growth would have occurred. Isotropic grain growth during straining would result in an under-estimate of e_g, while preferential grain growth in particular directions could lead to an error in either direction.

(2) Inhomogeneous deformation. Measurements were made in the centre of the specimen, where the strain is higher than the average strain in the specimen. This leads to an over-estimate of the measured value of e_g relative to the average strain e_g over the entire specimen.

The measured amount of shortening e_g, as inferred from grain flattening, is compared with the known total amount of shortening in the specimen (e_t) and Fig. 8 shows the ratios e_g/e_t for data points plotted in a log strain rate vs. log stress graph. It can be seen that in flow regimes 1 and 2 the average aspect ratio of grains reflects nearly the total strain imposed (average ratio e_g/e_t 0.92) whereas in the superplastic flow regime 3 only a third of the strain applied is reflected in grain flattening (average e_g/e_t 0.34). The transition from high to low ratios e_g/e_t almost ideally coincides with the transition into the superplastic flow regime as inferred from the rheological data (stippled line in Fig. 2). Within the flow regime 3 there is a tendency for lower ratios e_g/e_t at lower stresses and higher temperatures.

These results suggest that intracrystalline plasticity is dominating in flow regimes 1 and 2 and that some other mechanism such as grain-boundary sliding provides roughly two-thirds of the total strain in regime 3. A definite conclusion that grain-boundary sliding occurred is not justified by these results alone because strongly preferential grain-boundary migration in a direction parallel to the axis of shortening could theoretically be envisaged as occurring simultaneously with intracrystalline plasticity. The prime evidence for grain-boundary sliding will be presented next.

Scanning electron microscopy

The topographical relief on prepolished split cylinders deformed in regimes 2 and 3 is shown in Figs. 9a and b, respectively. It is evident that there is more relief in samples deformed in regime 3. Although the orientation of the contrast effects is dependent on the location of the electron detector relative to the specimen, the relief effects in Fig. 9 were observed for all orientations of the specimen. Measurements of step heights from stereo-pairs showed that the maximum vertical displacement v_{max} in regime 2 was about 1 μm while in regime 3 v_{max} it was about 5 μm.

An estimation of the strain e_{gbs} due to grain-boundary sliding was made in a region containing 50 grains (40 μm × 30 μm) in a superplastically deformed specimen (run 2802, 19.8% strain). The average vertical displacement $\overline{v_r}$ was 1.1 μm, giving e_{gbs} = 21%. This result shows that in this region of the specimen the total strain was accounted for by grain-boundary sliding. (The errors involved in the measurements are large. The greatest uncertainty arises in the measurement of the parallax, with an estimated 20%.) Also, from stereo viewing, it is apparent that the relief is variable. For example, in Fig. 9b the value of v_r between grains 1 and 2 was 5.5 ± 1 μm, while the v's for the groups 3, 4 and 5 were approximately zero. The problem of representative sampling is further illustrated in Fig. 9c, which is a lower magnification of

Fig. 9b. Region A delineates that used to measure e_{gbs}; it is apparent that some neighbouring regions show less relief, indicating a smaller proportion of e_{gbs}/e_{total}.

In a specimen (2674) deformed in regime 2, e_{gbs}/e_{total} is found to be about 20%. Fig. 9a shows that the grains in this specimen have undergone significantly more flattening than those in Fig. 9b.

Transmission electron microscopy

These observations were made primarily to compare the dislocation densities and substructural arrangements in specimens deformed in the high-n and low-n regimes. The undeformed material has a variable dislocation density. No free dislocations are present in some grains; others have up to 10 free dislocations within them, corresponding to a density of $5 \cdot 10^8$ cm^{-2}.

The results of the measurements of free dislocation density ρ for the deformed specimens are shown in Fig. 10. In this figure, the flow stress is plotted against $(\mu b)^2\rho$. The most obvious feature is the wide range of ρ-values in the superplastically deformed specimens compared with the smaller scatter in specimens from regime 2. Because of this variability it has been found more useful to characterize the differences between regimes 2 and 3 in terms of the dislocation configurations. The large spread in ρ in the superplastic field arises because there are two types of grains. One type has virtually no dislocations; the other type has extremely high densities, up to $7 \cdot 10^9$ cm^{-2}. The high-n specimens had a more uniform distribution of dislocations from grain to grain.

Since the SEM study clearly indicated the importance of grain-boundary sliding a careful study was undertaken to determine if there were any significant differences in the grain-boundary structures between regimes 2 and 3 or any "core—mantle" differences in the grains (Gifkins, 1974). No differences in grain-boundary structures were observed. Voids were observed along grain boundaries and at triple-point junctions but these were probably inherited from the starting material since there was no significant difference in the void distribution between undeformed and deformed specimens (whether in regime 2 or 3). There were no other microstructural features specific to the grain boundaries. Core—mantle features were observed, mainly consisting of subboundaries, but no differences between specimens deformed in regimes 2 and 3 were found.

In specimens deformed in regime 2 the free dislocations were distributed uniformly within the grains (Fig. 11a). Dipole and loop structures were observed. Where determined, the direction of the dominant Burgers vector was $\langle\bar{1}012\rangle$ in morphological Miller Bravais indices. But there is evidence that some dislocations have other Burgers vectors, both because they would be necessary to satisfy the requirement $\Sigma b_i = 0$ at nodal points and from contrast analysis.

In specimens deformed in regime 3, similar features were observed in the

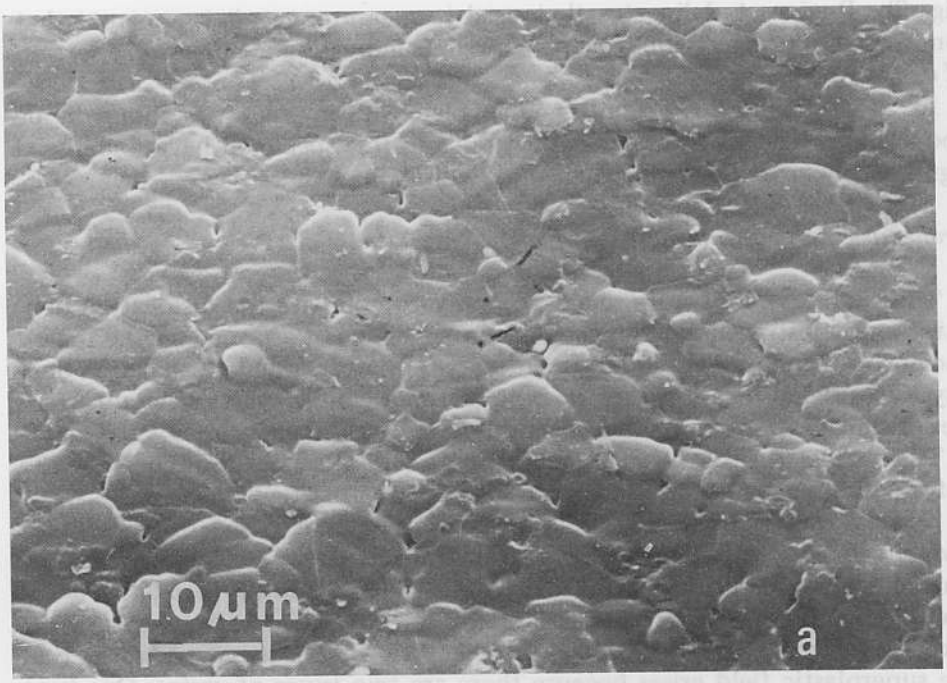
10 µm
a

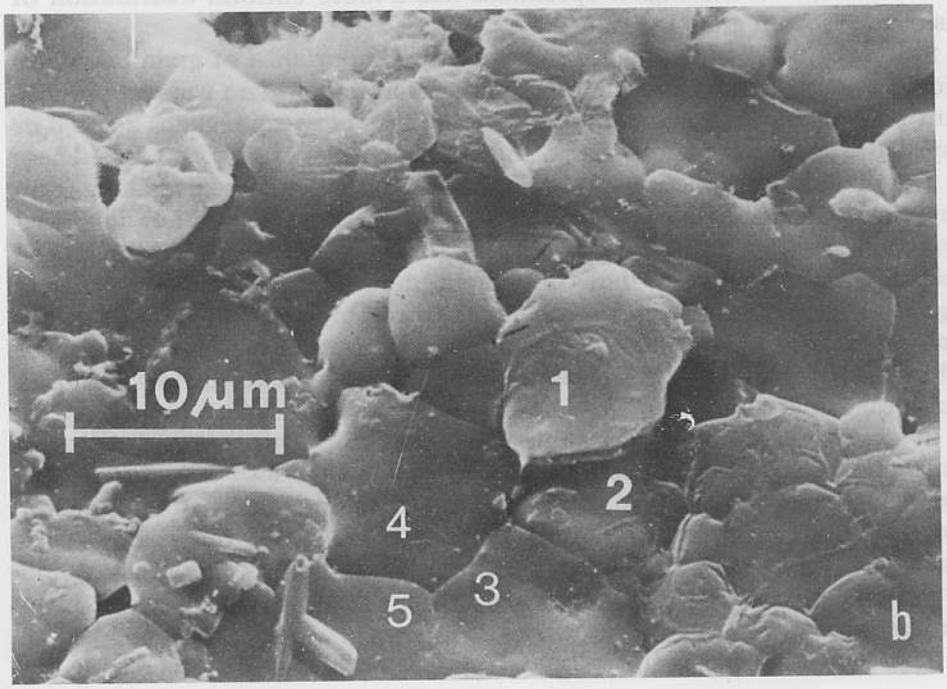
10 µm
1
2
3
4
5
b

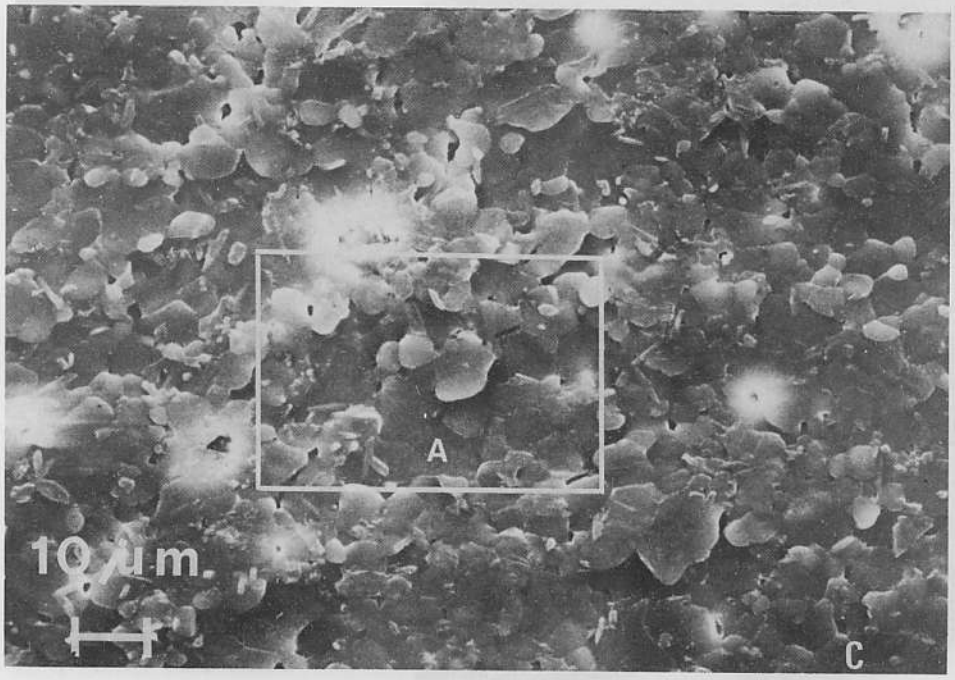

Fig. 9. Scanning electron micrographs of the surface of deformed split cylinders — shortening axis N—S. (a) Test 2674 deformed in regime 2 (30° tilt), 19.5% shortening (700°, 10^{-3} sec^{-1}), (b) Test 2802 deformed in regime 3 (30° tilt), 19.8% shortening (800°, 10^{-4} sec^{-1}). (c) Test 2802 (0° tilt).

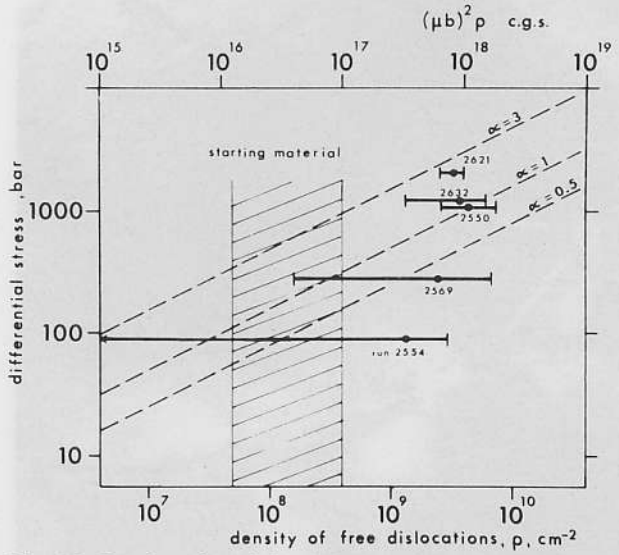

Fig. 10. Log-log plot of the dislocation density vs. the differential stress. Lines for various values of constant α in a relationship $\sigma = \alpha\mu b\rho^{1/2}$ are superimposed only for the purpose of comparison with the observations (μ = 0.25 Mbar, b = 6.3 Å).

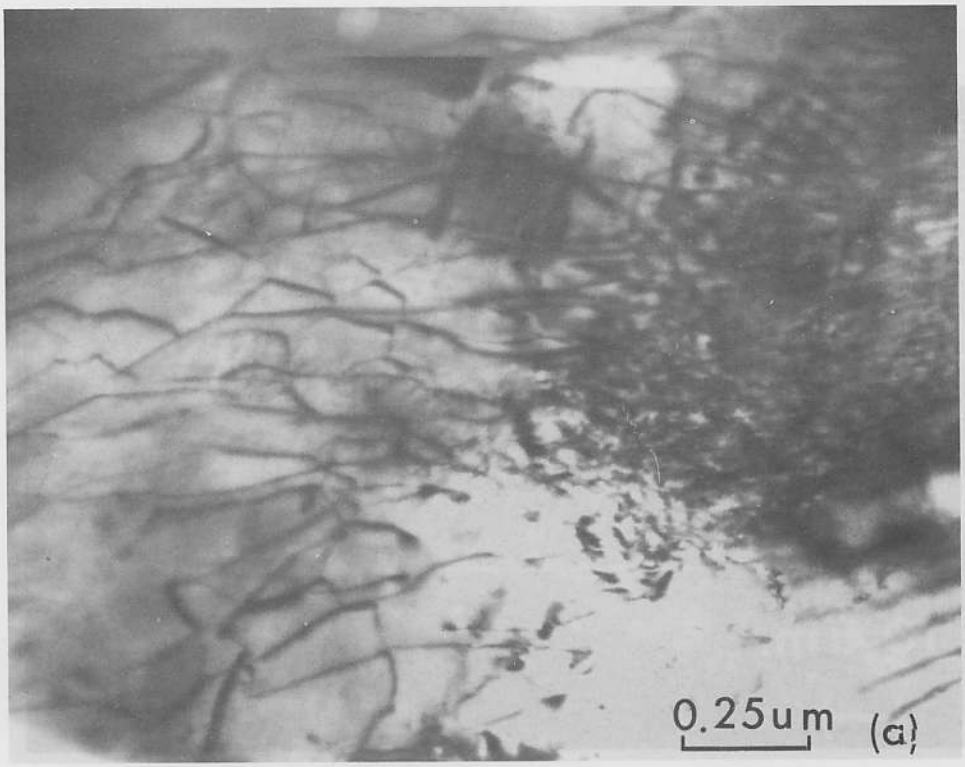
0.25um
(a)

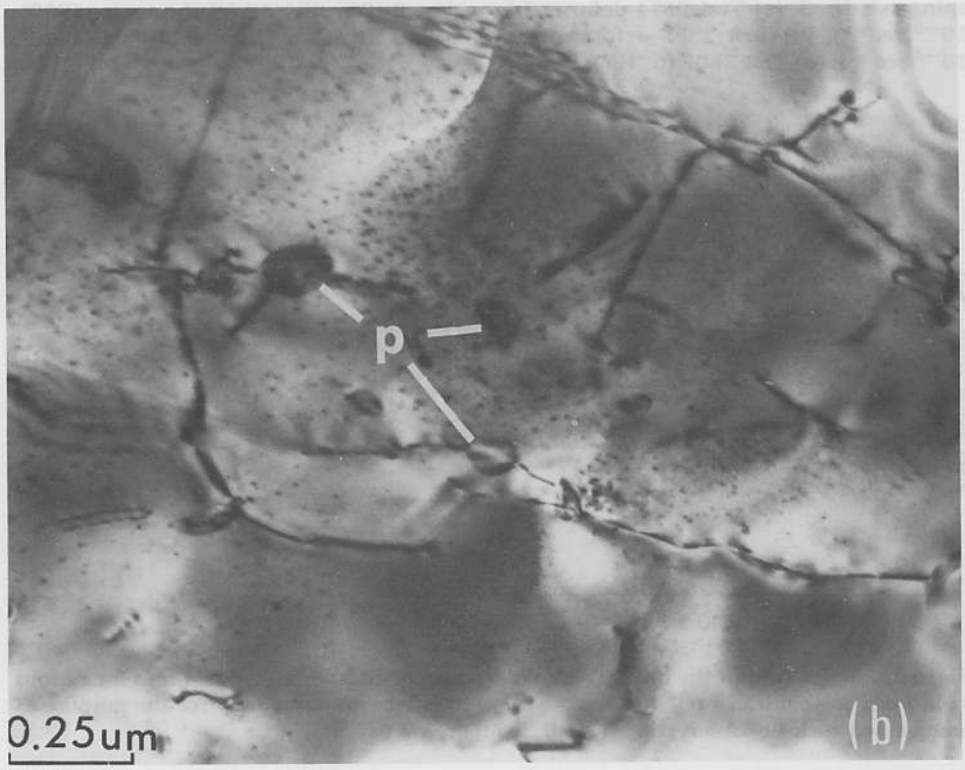
p
0.25um
(b)

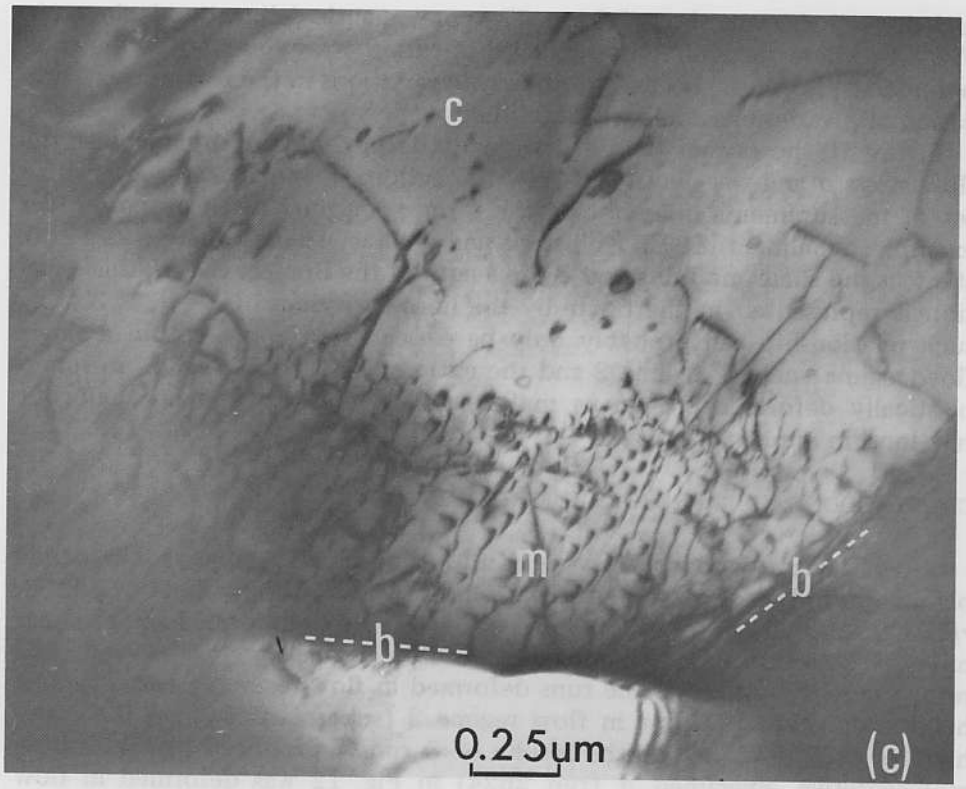

Fig. 11. Transmission-electron microscopy of the dislocation substructures. (a) Test 2550 deformed in regime 2, 12% shortening (600°, 10^{-5} sec^{-1}). (b) Test 2569 deformed in regime 3, 36% shortening (900°, $6.7 \cdot 10^{-4}$ sec^{-1}). (c) Test 2554 deformed in regime 3, 28% shortening (800°, 10^{-5} sec^{-1}); c = core region; m = mantle region; b = grain boundaries.

high-ρ grains. In the low-ρ grains, small precipitates were observed (marked p in Fig. 11b; note that the fine spots are the result of electron beam damage). These precipitates were not preferentially located at grain or subgrain boundaries and as can be seen in Fig. 11b, they did not appear to influence the dislocation distribution. The latter feature indicates that they do not contribute to a precipitation hardening effect nor do they act as substantial obstacles to grain-boundary sliding. The precipitates have not been identified.

There is direct evidence for subgrain or cell formation. In samples deformed in regime 2, the subgrains were commonly elongate (2 μm × 1 μm) although equidimensional subgrains about 1 μm or less were also observed. In superplastically deformed specimens, cells were also observed; in high-ρ grains the substructures were similar to those in regime-2 material. For low-ρ grains, the cell boundaries were clearly resolved into dislocation networks

and the cell size was about 2.5 μm. The core—mantle delineation is shown in Fig. 11c where the simple hexagonal dislocation array lies close to the grain boundaries; however, because of thickness variations in the foil no clear indication of ρ-variations could be established.

Figure 10 shows that there is no clearly defined relationship between the flow stress σ and the density of free dislocations ρ. In particular, the whole set of measurements does not fit the form $\sigma = \alpha\mu b\rho^{1/2}$ often proposed (for example, Smallman, 1970; Kohlstedt and Goetze, 1976), where α is a constant, μ the shear modulus and b the length of the Burgers vector; this equation is represented in the figure by the lines for values of $\alpha = \frac{1}{2}$, 1, 3. Any such relationship can probably only be expected to apply within a single flow regime such as regime 2 and the extreme scatter of ρ-values in superplastically deformed specimens makes any attempts to find an analogous relationship in regime 3 futile.

CRYSTALLOGRAPHIC PREFERRED ORIENTATION

X-ray transmission profiles were run for the following six crystallographic planes (morphological Miller-Bravais indices used throughout): $f(02\bar{2}1)$, $r(10\bar{1}1)$, $c(0001)$, $a(11\bar{2}0)$, $(44\bar{8}3)$ and $e(01\bar{1}2)$. Undeformed samples and nine specimens deformed in the various flow regimes were analyzed. The reproducibility within all the runs deformed in flow regimes 1 and 2 on one hand and within the runs in flow regime 3 (superplasticity) on the other hand is excellent, so that the results of 3 runs reproduced in Fig. 12 are representative. Specimen *A* (run 2624) in Fig. 12 was deformed in flow regime 2 up to 12% shortening, specimen *B* (run 2632) in the same flow regime up to 31% and specimen *C* (run 2606) in the superplastic flow regime 3 up to 29% shortening. The normalized profiles for undeformed Solnhofen limestone are superimposed (dashed lines). The angle χ is defined as the angle between the pole of the reflecting plane and the direction of shortening strain (e_3) in the case of the deformed specimens, the reference direction for the angle χ in the undeformed specimens is the normal to the bedding plane (the subsequent axis of shortening).

Specimens *A* and *B* illustrate the increase in the degree of preferred orientation (P.O.) with increasing strain. The main characteristics of the type of P.O. in flow regimes 1 and 2 are: (1) a main *c*-axis maximum at 90° to e_3, accentuating the pre-existent maximum in this plane, and a secondary maximum at 37° to e_3; (2) a point maximum of *a*-poles parallel to e_3 and a second concentration at 55° to e_3.

Although a rigorous conversion of the data in Fig. 12 into an inverse pole figure (Wenk et al., 1973) was not made, the profiles shown in Fig. 12 as well as the profiles for the *e*-plane and $(44\bar{8}3)$ are readily seen to be compatible with a main concentration of strain axes around the *a*-pole and a secondary concentration at 37° to *c*, near the *e*-pole (Fig. 13).

Specimen *C*, deformed superplastically, not only has a weaker P.O. than

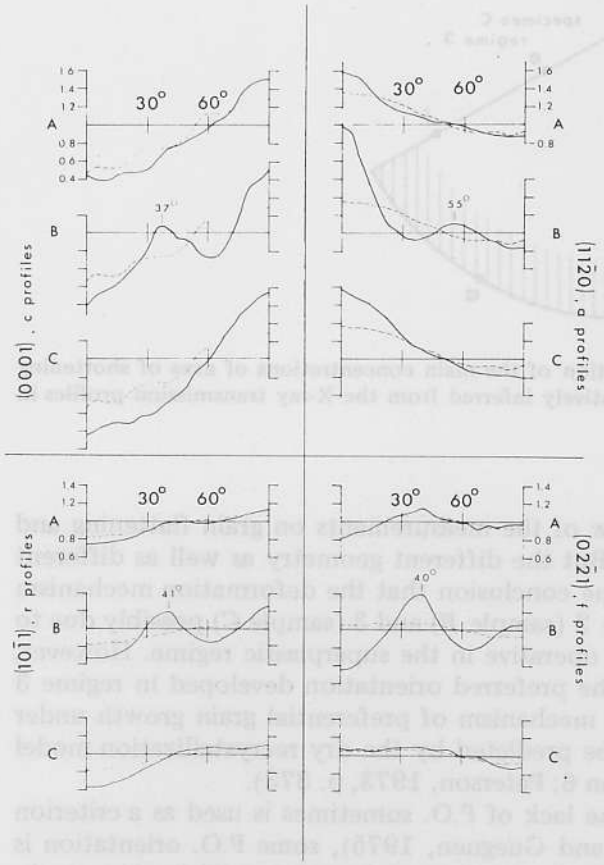

Fig. 12. Normalized X-ray transmission profiles for deformed specimens *A*, *B* and *C* (specimen *A*: 600°C, $3.5 \cdot 10^{-5}$ sec^{-1}; *B*: 700°C, $2.0 \cdot 10^{-3}$ sec^{-1}; *C*: 700°C, $1.4 \cdot 10^{-5}$ sec^{-1}) and the superimposed profiles (broken lines) of an undeformed specimen for various reflections. The angle χ plotted on a horizontal axis is defined as the angle between the pole of the reflecting planes and the direction of shortening or the normal to the bedding plane, respectively.

specimen *B* (at the same strain), but some of the characteristics of specimen *B* are missing: the secondary maxima in the *c*- and *a*-profiles disappear. The geometry of the P.O. is the same as the one in the undeformed limestone: in terms of an inverse pole figure the concentration of *c*-axes at 90° is maintained, but contrary to specimen *B* no concentration of the strain axes around the *a*-pole can be deduced and the secondary maximum of strain axes at 37° to *c* is also missing.

The fact that some preferred orientation occurs in superplastically deformed Solnhofen limestone suggests that intracrystalline plasticity contributes to some of the total strain achieved under superplastic conditions.

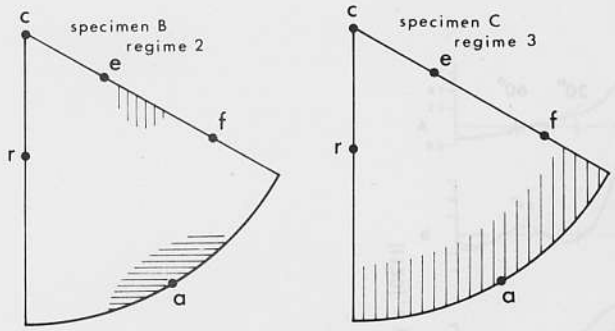

Fig. 13. Sketch showing the position of the main concentrations of axes of shortening in an inverse pole figure as qualitatively inferred from the X-ray transmission profiles in Fig. 12.

This is not surprising, in view of the measurements on grain flattening and the results of TEM studies. But the different geometry as well as different intensity in P.O. reinforces the conclusion that the deformation mechanism changes between flow regime 2 (sample *B*) and 3 (sample *C*) possibly due to different glide systems being operative in the superplastic regime. However, it cannot be excluded that the preferred orientation developed in regime 3 arises at least in part from a mechanism of preferential grain growth under stress; the same P.O. would be predicted by the dry recrystallization model of Kamb (Kamb, 1959, section 6; Paterson, 1973, p. 373).

In spite of the fact that the lack of P.O. sometimes is used as a criterion for superplasticity (Boullier and Gueguen, 1975), some P.O. orientation is not unusual in other superplastically deformed materials (Edington et al., 1976).

It is not possible at this stage to speculate on the glide systems responsible for the preferred orientations observed. It can only be said that the type of P.O. observed in all the flow regimes is incompatible with twinning as a major deformation mechanism. Twinning tends to move the axes of shortening towards the *c*-axis (Turner and Weiss, 1963, p. 347). This conclusion is consistent with the observation that twinned grains in Solnhofen limestone are extremely rare at all deformation conditions reported here.

The results obtained on specimen *B* agree with pole figures obtained from experimentally deformed Solnhofen limestone as published by Kern (1971, Fig. 7, axially symmetric strain field, 650°C). All the specimens analyzed show a fundamentally different type of P.O., however, when compared with the results of Wenk et al. (1973) as described for Solnhofen limestone, deformed at similar temperatures and strain rates. Wenk et al. (1973) found a concentration of stress axes in an inverse pole figure around *c* or *e* and at higher temperatures around *r*. In none of their runs is a concentration at 90° to the *c*-axis reported. Since at least some of their runs were made at similar

confining pressures, the reason for this discrepancy is not known, but might be due to the different constraints in the solid medium apparatus. It is noteworthy that twinning is extensively developed in their specimens (Barber and Wenk, 1973).

DISCUSSION

Deformation mechanisms

The observations on microstructure and crystallographic preferred orientation indicate that glide of dislocations plays a dominant role in flow regimes 1 and 2, while the amount of grain-boundary sliding is relatively small, and twinning plays no significant role at all. The transition from regime 1 with an exponential stress-dependence of strain rate into regime 2 characterized by high n-values in a power-law relationship between stress and strain rate is not well understood; the microstructural or textural observations do not indicate any significant change in deformation mechanisms across this transition. In both flow regimes steady-state behaviour is achieved after a few percent strain and in both creep is thermally activated with an apparent activation energy for creep not far below the experimentally determined activation energy for diffusion of carbon and oxygen in calcite (88 kcal mole^{-1}, Anderson, 1969; for the apparent activation energy of creep in flow regime 1 see Rutter and Schmid, 1975). This correspondence in activation energy suggests that a bulk diffusional process is the rate-controlling step for glide; in particular it is consistent with the glide being climb-controlled, as is often proposed for "dislocation creep" (Stocker and Ashby, 1973a). Further, the value of $n = 4.7$ is close to that predicted, $n = 4.5$, for creep by climb-controlled glide by Weertman (1975). When the constitutive equation in regime 2 is written in the form proposed by Dorn (Mukherjee et al., 1969), the Dorn parameter is equal to $2 \cdot 10^7$ for a shear modulus of $0.25 \cdot 10^6$ bars and an average Burgers vector of $6.3 \cdot 10^{-8}$ cm (using the diffusion data of Anderson, 1969, at 700°C); this falls within the range of values for other materials in the plot of Dorn parameter versus the parameter n given by Stocker and Ashby (1973b).

The flow regime 3 is best characterized as a regime of superplastic flow because it has the following properties, in common with superplastic flow in metals:

(1) A low value of the stress exponent n implies a high strain-rate sensitivity of the flow stress and characterizes the rheological behaviour.

(2) A strong grain-size dependence of strain rate is observed ($\dot{\varepsilon} \propto d^{-b}$, where $b \sim 3$).

(3) The apparent activation energy for creep is substantially less than the experimentally determined activation energy for C and O self-diffusion in calcite and also significantly less than the apparent activation energy for creep observed in flow regime 2.

(4) The amount of grain flattening corresponds to only a portion ($\frac{1}{3}$) of the total strain applied.

(5) Grain-boundary sliding observed microscopically accounts for approximately two-thirds of the strain.

Not all these aspects of superplastic flow rule out diffusional flow models. The observations that the value of the stress exponent n is never as low as unity and that the grain shape does not reflect the strain as it should in an essentially intracrystalline deformation mechanism, however, are not consistent with models such as Nabarro-Herring and Coble creep; also grain-boundary sliding plays only a secondary role in the diffusional models, corresponding to much less activity than that observed. On the other hand, the observed flow behaviour corresponds well with that expected for grain-boundary sliding mechanisms.

We therefore conclude that the deformation mechanism in the superplastic regime is one dominated by grain-boundary sliding, that is, by the relative movement of grains rather than by intracrystalline processes, although some intracrystalline deformation evidently occurs as a subordinate process. Grain-boundary sliding cannot occur in isolation because of accommodation difficulties at irregularities in the grain boundaries and, especially, at the junctions where more than two grains meet. Two types of accommodation are in principle possible, involving firstly the diffusion of material as required for the accommodation, including grain-boundary diffusion and, secondly, the plastic deformation of grains. The models of Ashby and Verrall (1973) and Mukherjee (1975) represent these two possibilities and are taken here as giving the types of dependence on experimental variables that may be expected.

Ashby and Verrall's model of creep by diffusion—accommodation grain-boundary sliding leads to the constitutive equation:

$$\dot{\epsilon} = \frac{K' D_{\mathrm{eff}} G V}{kTd^2} \left(\frac{\sigma}{G}\right) \tag{3}$$

The effective diffusivity $D_{\mathrm{eff}} = D_{\mathrm{v}}(1 + 3.3\ \delta D_{\mathrm{gb}}/dD_{\mathrm{v}})$, usually reduces to $3.3\ \delta D_{\mathrm{gb}}/d$ when the grain boundary diffusivity, D_{gb}, is much higher than the bulk diffusivity D_{v}, giving:

$$\dot{\epsilon} = \frac{3.3 K' \delta G V D_{\mathrm{gb}}}{kTd^3} \left(\frac{\sigma}{G}\right) \tag{4}$$

where K' is a constant (~ 100), V the atomic volume, G the shear modulus, δ the width of the grain boundary effective in the diffusional flow, k the Boltzmann's constant and d the grain size.

Mukherjee's model of creep by grain-boundary sliding with accommodation by dislocation creep within the grains gives the constitutive equation:

$$\dot{\epsilon} = \frac{K'' D_{\mathrm{gb}} G b}{kT} \left(\frac{b}{d}\right)^2 \left(\frac{\sigma}{G}\right)^2 \tag{5}$$

where K'' is a constant (~ 2) and b the Burgers vector.

Since the grain-boundary diffusivity has not been measured experimentally the predicted creep rates cannot be calculated directly for comparison with our measurements. However, it is to be noted that, since the activation energy of grain-boundary diffusion is usually one half or two-thirds the value of the bulk diffusivity, the predicted temperature-dependence of the strain rate would roughly correspond to that observed. The predicted values of $n = 1$ in eq. 4 and $n = 2$ in eq. 5 bracket the observed value of 1.7, while the predicted grain-size dependence in eq. 4 may fit the observations better, but such a fit cannot be given much weight. We conclude that on the present evidence no clear distinction can be drawn between the models discussed here.

The strong variation in dislocation density from grain to grain suggests that some grains have undergone more intracrystalline deformation than others. This effect may be a result of dislocation creep competing successfully with grain-boundary sliding in those grains most favourably oriented for slip; the bulk aggregate would then deform by the superposition of two relatively independent and additive deformation mechanisms, grain-boundary sliding and dislocation creep. Such a mixed deformation process could also explain the observed decrease in n-values with decreasing stress (Fig. 5) as the relative contribution of dislocation creep decreased. An alternative explanation of the different dislocation densities from grain to grain is that these densities represent different stages in a cyclic recrystallization like those observed in the hot-working of metals (McQueen and Jonas, 1975). This alternative seems unlikely to apply here because no features have been observed that resemble nuclei or intermediate growth stages of a recrystallization process. Further study of the occurrence of strong variation in dislocation densities is desirable since if it could be shown to be characteristic of one or more of the mechanisms of superplastic flow it may be a useful diagnostic feature for recognizing that a rock has been deformed in a superplastic regime or even of distinguishing the principal mechanism of the deformation.

Tectonophysical significance

The applications of knowledge gained in laboratory experiments to natural tectonics have so far concerned situations where intracrystalline plasticity predominates. The microstructures and textures in a wide variety of rocks indicate indeed an important role of dislocation creep in many geological environments.

In the case of alternative flow regimes involving diffusional creep or intergranular creep it is much more difficult to establish good microstructural and textural criteria for these processes. Grain-boundary sliding and diffusional mass transfer do not normally leave obvious traces to be revealed by conventional microstructural techniques in natural tectonites. Elliott (1973)

has proposed criteria for recognizing diffusional creep, while Boullier and Gueguen (1975) have proposed criteria for superplasticity, applying these to interpret the microfabric of mylonites in peridotite nodules, anorthosites and amphibolites as indicating superplastic flow. No cases of superplasticity have yet been inferred in naturally deformed calcite rocks but the fine-grained calcite mylonite (equiaxed grains of around 1 μm) from the Glarus overthrust in the Swiss Alps (Schmid, 1975) is currently being studied from this point of view.

Most of the criteria for superplastic flow mentioned in this study are not directly applicable to a geologically deformed specimen. Potentially useful criteria are: (1) observation of approximately equiaxed grains in a tectonite known from independent evidence to have undergone large strains, where postkinematic annealing recrystallization can be excluded; and (2) evidence that finer grained domains have deformed more easily than coarser grained domains in a mineralogically homogeneous rock. The second criterion implies a grain-size sensitivity of flow incompatible with dislocation creep although equally well explained by diffusional creep. The large differences in dislocation density observed from grain to grain in the superplastic regime of Solnhofen limestone would also provide a practically useful criterion for recognizing superplastic flow if this effect could be shown to be a general one.

On the other hand, a very fine grain size (less than 10 μm has been suggested on the basis of laboratory studies in other materials) cannot be sustained as a necessary condition for superplastic flow (Fig. 14, to be discussed below). Nor is the absence of preferred orientation or a very low dislocation density; these criteria, proposed by Boullier and Gueguen (1975) and Schmid (1976), are not fulfilled by the present study and may therefore not be of general use.

Superplastic flow has not yet been widely discussed in a tectonophysical context, presumably because of the paucity of direct evidence so far for its occurrence. It is therefore of value to infer its range of significance by extrapolating the experimentally derived constitutive equations to geologically realistic stresses, strain rates and temperatures.

Ashby (1972) introduced the concept of a "deformation mechanism map". This is a valuable aid in carrying out extrapolations from one set of conditions to another because it provides a basis for delineating the limits for particular flow regimes within which given constitutive equations are valid. Ashby's maps are plotted in a flow stress versus temperature space for a given grain size, with superimposed contours of constant strain rate. More recently, Langdon and Mohamed (1976) have introduced an analogous procedure of plotting the deformation fields in a flow stress versus grain size space for a given temperature, again with superimposed contours of constant strain rate. The latter procedure is especially useful for depicting the role of grain size and is used here.

At this point, a distinction has to be made between a deformation-mecha-

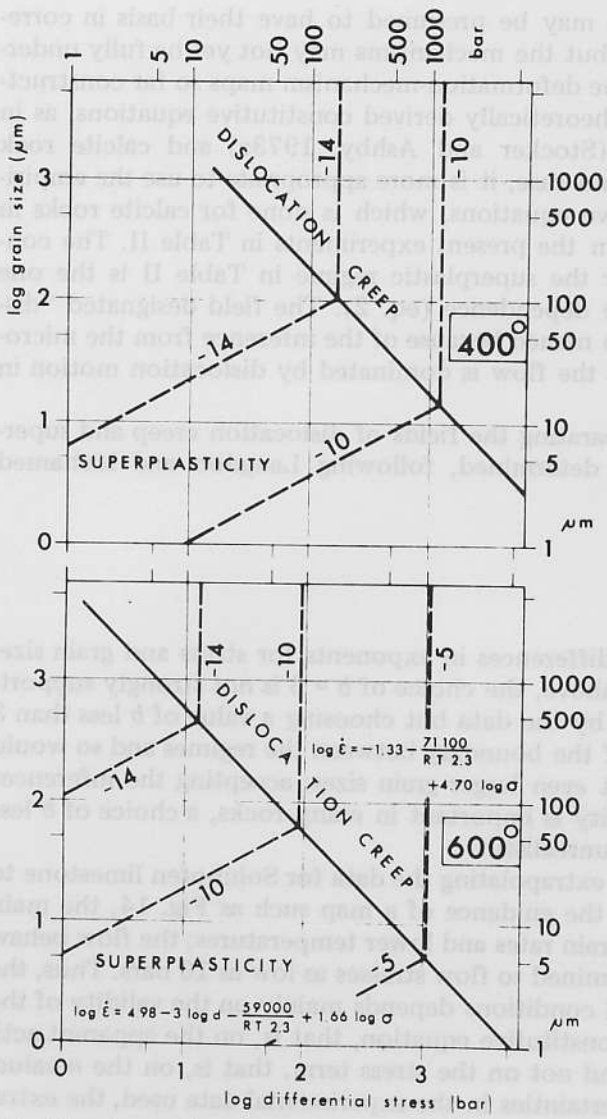

Fig. 14. Flow-regime maps at constant temperature (400°C and 600°C) in stress—grain-size coordinates. The maps are based on an extrapolation of the constitutive equations listed in Table II (the constitutive equation for superplastic flow has been expanded into eq. 2 to allow for $\dot{\varepsilon} \propto d^{-b}$) into geologically realistic strain rates. Broken lines: strain rate contours.

nism map per se, as used in metallurgy with the primary aim of depicting the conditions for appearance of given deformation mechanisms, and a map of the regimes of flow characterized primarily by their constitutive equations and the appearance of accompanying microstructural and textural diagnostic

criteria; these flow regimes may be presumed to have their basis in corresponding mechanism fields but the mechanisms may not yet be fully understood. In the former case, the deformation-mechanism maps so far constructed have relied heavily on theoretically derived constitutive equations, as in the case of olivine rock (Stocker and Ashby, 1973a) and calcite rock (Rutter, 1976). In the second case, it is more appropriate to use the empirically determined constitutive equations, which is done for calcite rocks in Fig. 14 using the data from the present experiments in Table II. The constitutive equation used for the superplastic regime in Table II is the one incorporating the grain-size dependence (eq. 2). The field designated "dislocation creep" has been so named because of the inference from the microstructural observations that the flow is dominated by dislocation motion in the grains.

The slope of the line separating the fields of dislocation creep and superplastic flow in Fig. 14 is determined, following Langdon and Mohamed (1976), by:

$$\frac{\mathrm{d}(\log d)}{\mathrm{d}(\log \sigma)} = \frac{\Delta n}{\Delta b}$$

where Δn and Δb are the differences in exponents for stress and grain size, respectively. As discussed above, the choice of $b = 3$ is not strongly supported in preference to $b = 2$ by the data but choosing a value of b less than 3 would steepen the slope of the boundary between the regimes and so would favour superplastic flow at even larger grain sizes; accepting the inferences that intracrystalline plasticity is important in many rocks, a choice of b less than 3 would appear to be unrealistic.

It is to be noted that in extrapolating the data for Solnhofen limestone to geological conditions with the guidance of a map such as Fig. 14, the main extrapolation is to lower strain rates and lower temperatures; the flow behaviour has already been determined to flow stresses as low as 10 bars. Thus, the extrapolation to geological conditions depends mainly on the validity of the temperature term in the constitutive equation, that is, on the apparent activation energy for creep, and not on the stress term, that is, on the n-value.

Although there are uncertainties in the experimental data used, the extrapolation in Fig. 14 suggests that:

(1) At geologically realistic strain rates between 10^{-10} and 10^{-14} sec^{-1}, the regime of superplastic flow broadens to encompass a wider range of grain sizes, extending to grain sizes much greater than 10 μm. The maximum grain size for superplasticity depends on the differential stress but can exceed 100 μm under some conditions. The transition into superplastic flow also occurs at larger grain sizes at higher temperatures, as shown by the 600° C and 400° C plots in Fig. 14.

(2) The flow stresses expected in this interval of strain rates are less than about 1300 bars at 400° C and less than about 100 bars at 600° C, regardless

of the deformation mechanism. The actual flow stress at any given strain rate (or strain rate at given stress) is very sensitive to grain size in the superplastic regime; extremely low flow stresses can be expected at grain sizes less than 10 μm (for example, 3 bars at 600°C at the geologically fast strain rate of 10^{-10} sec^{-1}).

The principal characteristics of the plots in Fig. 14 also suggest the following conclusions of a more general nature:

(1) A grain size of less than 10 μm is not a necessary condition for superplastic flow to occur in geologically deformed rocks.

(2) In a mineralogically homogeneous rock suite with varying grain size, competence contrasts may arise reflecting differences in flow resistance and ductility. Thus, an experimental study of an oolitic limestone revealed inhomogeneous strain associated with differences in grain size between ooids and matrix (Schmid and Paterson, 1977).

(3) Superplastic flow may be widespread in mylonites; it has already been proposed for olivine-rich mylonites by Boullier and Gueguen (1975). A grain-size reduction by syntectonic recrystallization can be envisaged as a preliminary development, leading in the course of large deformations to a stable zone of weakness within coarser grained country rock (White, 1976); the inverse grain-size dependence of superplastic flow may be an essential factor in stabilizing this situation.

(4) Assuming that superplastic flow can be demonstrated experimentally in olivine-rich rock and that this too will have characteristics analogous to those of the calcite rocks, superplastic flow at extremely low stresses at high temperatures must be considered as a serious possibility in the upper mantle, where so far only flow by dislocation creep and diffusional creep have been considered (Stocker and Ashby, 1973; Weertman and Weertman, 1975).

ACKNOWLEDGEMENTS

We thank T. Fitch for his help in computer work. We had profitable discussions with I. Allison, R. Coe, E.H. Rutter, S. White and many others. G. Milburn and T. White assisted in maintaining the apparatus and P. Willis provided us with excellent thin sections and technical assistance on the electron microscope.

REFERENCES

Anderson, T.F., 1969. Self diffusion of carbon and oxygen in calcite by isotope exchange with carbon dioxide. J. Geophys. Res., 74: 3918—3931.

Ashby, M.F., 1972. A first report on deformation mechanism maps. Acta Metall., 20: 887—897.

Ashby, M.F. and Verrall, R.A., 1973. Diffusion-accommodated flow and superplasticity. Acta Metall., 21: 149—163.

Baker, D.W., Wenk, H.R. and Christie, J.H., 1969. X-ray analysis of preferred orientation in finegrained quartz aggregates. J. Geol., 77: 144—172.

Barber, D.J., 1970. Thin foils of non-metals made for electron microscopy by sputter etching. J. Mater. Sci., 5: 1—8.

Barber, D.J. and Wenk, H.R., 1973. The microstructure of experimentally deformed limestone. J. Mater. Sci., 8: 500—508.

Boullier, A.M. and Gueguen, Y., 1975. Origin of some mylonites by superplastic flow. Contrib. Mineral. Petrol., 50: 93—104.

Boyde, A., 1970. Practical problems and methods in the three-dimensional analysis of scanning electron microscope images. In: Scanning Electron Microscopy. IIT Research Institute, Chicago, p. 107—112.

Carter, N.L., 1975. High-temperature flow of rocks. Rev. Geophys. Space Phys., 13: 344—349.

Edington, J.W., Melton, K.N. and Cutler, C.P., 1976. Superplasticity. Progr. Mater. Sci., 1: 61—158.

Elliott, D., 1973. Diffusion flow laws in metamorphic rocks. Geol. Soc. Am. Bull., 84: 2645—2664.

Gifkins, R.C., 1974. Hot and Strong. J. Aust. Inst. Metals, 19: 149—160.

Gillespie, P., McLaren, A.C. and Boland, J.N., 1971. Operating characteristics of an ion-bombardment apparatus for thinning non-metals for transmission electron microscopy. J. Mater. Sci., 6: 87—89.

Hale, K.F., 1974. Quantitative electron microscopy. In: T. Mulney and R.K. Webster (Editors), Modern Physical Techniques in Materials Technology. Oxford University Press, Oxford, p. 129—147.

Heard, H.C., 1963. Effects of large changes in strain rate in the experimental deformation of Yule marble. J. Geol., 71: 162—195.

Heard, H.C. and Raleigh, C.B., 1972. Steady-state flow in marble at 500—800°C. Geol. Soc. Am. Bull., 83: 935—956.

Kamb, W.B., 1959. Theory of preferred orientation developed by crystallization under stress. J. Geol., 67: 153—170.

Kern, H., 1971. Dreiaxiale Verformungen an Solnhofen Kalkstein im Temperaturbereich von 20—650°C. Röntgenographische Gefügeuntersuchungen mit dem Texturgoniometer. Contrib. Mineral. Petrol., 31: 39—66.

Kirby, S.H. and Raleigh, C.B., 1973. Mechanisms of high-temperature, solid-state flow in minerals and ceramics and their bearing on the creep behaviour of the mantle. Tectonophysics, 19: 165—194.

Kohlstedt, D.L. and Goetze, C., 1976. The dislocation structure of experimentally deformed marble. EOS Trans. A.G.U., 57: 327 (abstract).

Kohlstedt, D.L., Goetze, C. and Durham, W.B., 1976. Experimental deformation of single crystal olivine with application to flow in the mantle. In: S.K. Runcorn (Editor), Petrophysics: The Physics and Chemistry of Minerals and Rocks. Wiley, London.

Langdon, T.G., 1976. Grain boundary deformation processes. In: R.C. Bradt and R.E. Tressler (Editors). Deformation of Ceramic Materials. Plenum, New York, p. 101—126.

Langdon, T.G. and Mohamed, F.A., 1976. Deformation mechanism maps for ceramics. J. Mater. Sci., 11: 317—327.

McQueen, H.J. and Jonas, J.J., 1975. Recovery and recrystallization during high temperature deformation. In: Treatise on Materials Science and Technology, 6. Academic Press, New York, p. 393—493.

Means, W.D. and Paterson, M.S., 1966. Experiments on preferred orientation of platy minerals. Contrib. Mineral. Petrol., 13: 108—133.

Mukherjee, A.K., 1975. High-temperature creep. In: R.J. Arsenault (Editor), Treatise on Materials Science and Technology, 6. Academic Press, New York, p. 163—224.

Mukherjee, A.K., Bird, J.E. and Dorn, J.E., 1969. Experimental correlations for high-temperature creep. Trans. ASM, 62: 155—179.

Olsson, W.A., 1974. Grain size dependence of yield stress in marble. J. Geophys. Res., 79: 4859—4862.

Paterson, M.S., 1970. A high-pressure high-temperature apparatus for rock deformation. Int. J. Rock Mech. Min. Sci., 7: 517—526.
Paterson, M.S., 1973. Non-hydrostatic thermodynamics and its geological applications. Rev. Geophys. Space Phys., 11: 355—389.
Paterson, M.S., 1976a. Some current aspects of experimental rock deformation. Philos. Trans. R. Soc. London, Ser., A, 283: 163—172.
Paterson, M.S., 1976b. Experience with an internally heated gas-medium deformation apparatus to 500 MPa. 2nd Int. Conf. on High Pressure Engineering, Brighton, 1975, to be published by The Institution of Mechanical Engineers.
Petch, N.J., 1953. The cleavage strength of polycrystals. J. Iron Steel Inst., 174: 25—28.
Rutter, E.H., 1974. The influence of temperature, strain rate and interstitial water in the experimental deformation of calcite rocks. Tectonophysics, 22: 311—334.
Rutter, E.H., 1976. The kinetics of rock deformation by pressure solution. Philos. Trans. R. Soc. London, Ser. A, 283: 203—219.
Rutter, E.H. and Schmid, S.M., 1975. Experimental study of unconfined flow of Solnhofen limestone at 500°—600°C. Geol. Soc. Am. Bull., 86: 145—152.
Schmid, S.M., 1975. The Glarus overthrust: Field evidence and mechanical model. Eclogae Geol. Helv., 68: 251—284.
Schmid, S.M., 1976. Rheological evidence for changes in the deformation mechanism of Solnhofen limestone towards low stresses. Tectonophysics, 31: T21—T28.
Schmid, S.M. and Paterson, M.S., 1977. Strain analysis in an experimentally deformed oolitic limestone. To be published in: S.K. Saxena and S. Battacharji (Editors), Energetics of Geological Processes. Springer, Berlin.
Smallman, R.E., 1970. Modern Physical Metallurgy. Butterworths, London, Chapter 6.
Stocker, R.L. and Ashby, M.F., 1973a. On the rheology of the upper mantle. Rev. Geophys. Space Phys., 11: 391—426.
Stocker, R.L. and Ashby, M.F., 1973b. On the empirical constants in the Dorn equation. Scripta Metall., 7: 115—120.
Turner, F.J. and Weiss, L.E., 1963. Structural Analysis of Metamorphic Tectonites. McGraw-Hill, New York.
Weertman, J., 1968. Dislocation climb theory of steady-state creep. Trans. ASM, 61: 681--694.
Weertman, J., 1975. High-temperature creep produced by dislocation motion. In: J.C.M. Li and A.K. Mukherjee (Editors), Rate Processes in Plastic Deformation of Materials. ASM, Metals Park, Ohio, p. 315—336.
Weertman, J. and Weertman, J.R., 1975. High-temperature creep of rock and mantle viscosity. Ann. Rev. Earth Planet. Sci., 3: 293—315.
Wenk, H.R., Venkitasubramanyan, C.S. and Baker, D.W., 1973. Preferred orientation in experimentally deformed limestone. Contrib. Mineral. Petrol., 38: 81—114.
White, S., 1976. The effects of strain on the microstructures, fabrics and deformation mechanisms in quartzites. Philos. Trans. R. Soc. London, Ser. A, 283: 69—86.